ECCOMAS Congress 2016
VII European Congress on Computational Methods in Applied Sciences and Engineering
M. Papadrakakis, V. Papadopoulos, G. Stefanou, V. Plevris (eds.)
Crete Island, Greece, 5–10 June 2016

# A MESOSCALE STUDY OF DEFORMATION AND FAILURE OF ANGLE-PLY LAMINATES UNDER TENSILE LOADING BY MEANS OF NUMERICAL HOMOGENIZATION

**Marek Romanowicz**

Bialystok University of Technology, Department of Mechanical Engineering
ul. Wiejska 45C, 15 351 Bialystok, Poland
e-mail: m.romanowicz@pb.edu.pl

**Keywords:** numerical homogenization, polymer-matrix composites, finite element analysis.

**Abstract.** *A multi-ply unit cell model for predicting the tensile response of a ±45 angle-ply laminate based on the finite element method is presented. Two different interfiber failure mechanisms leading to matrix cracking are reproduced in the simulations by using appropriate constitutive equations. The effect of fiber-to-fiber interaction within the ply is incorporated in the model by applying a hexagonal array of fibers. The predictions from this model are compared with experimental data available in the literature, and are found to be in good agreement.* .

## 1 INTRODUCTION

Recently, researchers have shown an increased interest in studying the deformation and failure of composite laminates by using multi-ply unit cell models [1-8]. In the present paper, the mesoscale approach based on a rhombohedral unit cell proposed by Zhang et al. [6] is extended. This approach is based on an assumption that the structure of the whole laminate can be idealized at the ply scale as a periodic array of repeated unit cells. Some new issues, like fiber/matrix interface debonding, development of plastic strain in the matrix and hexagonal fiber packing are introduced in the mesoscale model of a ±45 angle-ply laminate. The objective of this paper is to show that an analysis of local stresses in the mesoscale model is capable of identifying the failure mechanism and predicting the tensile behavior of a ±45 angle-ply laminate.

## 2 MESOSCALE FINITE ELEMENT MODEL

As shown in Fig.1, two coordinate systems are used to analyze angle-ply laminates. The first one is a orthogonal coordinate system ($x_1$–$x_2$–$x_3$), which is used to determine the direction of loading. The second one is a skew coordinate system ($x_1^s$–$x_2^s$–$x_3^s$), which is used to define the unit cell geometry. This coordinate system is set up such that the $x_1^s$ and $x_2^s$ axes lie in the plane of the laminate along the fiber directions and the $x_3^s$ axis is perpendicular to it. It should be noted that the fiber orientation angle θ is measured with respect to the $x_1$ axis of the orthogonal coordinate system. A unit cell of an angle-ply laminate consists of three rhombohedrons which represent three successive plies with various fiber orientations. The structure of an ±θ angle–ply laminate can be viewed at the ply scale in the skew coordinate system ($x_1^s$–$x_2^s$–$x_3^s$) as a periodical array of plies containing a periodic subarray of fibers. Thus, a unit cell of an angle-ply laminate is built with unit cells of plies. In this study, the fibers are distributed uniformly throughout the ply in the form of a hexagonal array.

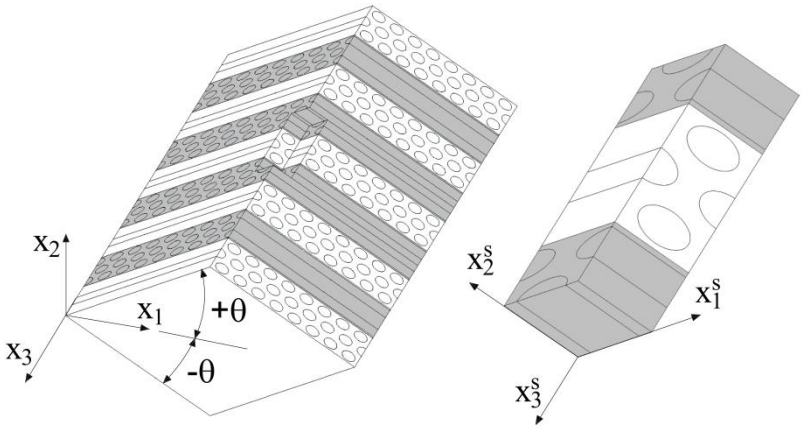


Figure. 1: Geometry of a rhombohedral unit cell.

In this paper, 3-D multi-ply mesoscale models of a ±45$^o$ angle-ply laminate subjected to tension along the $x_2$ direction are examined. The material properties of fibers and matrix (Table 1) correspond to those reported in the World Wide Failure Exercise [9] for Silenka E-glass 1200tex fibers and MY750/HY917 epoxy matrix. The dimensions of rhombohedral unit cells were chosen so as to accommodate the radius of fiber $r_f$ = 8 μm, and to respect the fiber volume content $V_f$ = 60%. The full rhombohedrons were meshed with three–dimensional eight–node elements (SOLID185) and solved by using Ansys finite element code [10].

| Silenka E-glass fiber | | | MY750/HY917/DY063 epoxy matrix | | | | | |
|---|---|---|---|---|---|---|---|---|
| $E_f$ [GPa] | $\nu_f$ | $X_f$ [MPa] | $E_m$ [GPa] | $\nu_m$ | $k$ [MPa] | $\mu$ | $Y_m$ [MPa] | $S_m$ [MPa] |
| 74 | 0.2 | 2150 | 4.5 | 0.35 | 43.35 | 0.1 | 100 | 87 |

| fiber/matrix interface | | | | | |
|---|---|---|---|---|---|
| $k_n$ [GPa/m] | $k_t$ [GPa/m] | $G_n^c$ [J/m$^2$] | $G_t^c$ [J/m$^2$] | $\sigma_n^c$ [MPa] | $\tau_t^c$ [MPa] |
| 0.1x10$^9$ | 0.1x10$^9$ | 15 | 30 | 15 | 30 |

Table 1: Mechanical properties of the lamina constituents.

## 2.1 Numerical homogenization

Periodic deformation of the rhombohedral unit cell is controlled by macroscopic strains by using the following boundary conditions [11]

$$\begin{aligned} u_i^s(a_1, x_2^s, x_3^s) - u_i^s(-a_1, x_2^s, x_3^s) &= 2a_1\varepsilon_{i1}^s, \\ u_i^s(x_1^s, a_2, x_3^s) - u_i^s(x_2^s, -a_2, x_3^s) &= 2a_2\varepsilon_{i2}^s, \\ u_i^s(x_1^s, x_2^s, a_3) - u_i^s(x_1^s, x_2^s, -a_3) &= 2a_3\varepsilon_{i3}^s, \end{aligned} \tag{1}$$

where $i$ = 1, 2, 3, and $2a_1$, $2a_2$, $2a_3$ are the dimensions of the unit cell in the skew coordinate system, $\varepsilon_{ij}^s$ are the components of the applied strain in the skew coordinate system. In order to apply the periodic boundary conditions to the finite element model, the displacements in the skew coordinate system $u_1^s$, $u_2^s$, $u_3^s$ must be rewritten in terms of the displacements in the orthogonal coordinate system $u_1$, $u_2$, $u_3$ by using the following relationships [11]

$$\begin{Bmatrix} u_1^s \\ u_2^s \\ u_3^s \end{Bmatrix} = \frac{1}{\sin 2\theta} \begin{bmatrix} \sin\theta & -\cos\theta & 0 \\ \sin\theta & \cos\theta & 0 \\ 0 & 0 & \sin 2\theta \end{bmatrix} \begin{Bmatrix} u_1 \\ u_2 \\ u_3 \end{Bmatrix}. \tag{2}$$

The components of macroscopic stress corresponding to the applied strain can be calculated from

$$\bar{\sigma}_{ij} = \frac{1}{V}\int_V \sigma_{ij}\, \mathrm{d}V \tag{3}$$

where $V$ is the volume of the rhombohedral unit cell.

## 2.2 Constitutive equations of matrix and interface

The epoxy matrix is modeled within the framework of the finite deformations as a elasto–plastic solid which hardens isotropically. The deformation of polymeric materials is highly sensitive to the hydrostatic pressure and plastic flow of these materials can exhibit plastic dilatancy. To address this requirement, the Drucker–Prager plasticity model [12], which incorporates the linear dependence on the hydrostatic stress, is used. In terms of the first invariant of stress $I_1$ and the second invariant of the deviatoric part of stress $J_2$, the yield function is given as

$$\mathrm{f} = (\mu\, I_1 / 3) + \mathrm{sqrt}(J_2) - k\,, \tag{4}$$

where $\mu$ is the pressure sensitivity factor, $k$ is the flow stress of the material under pure shear. Experiments showed that the pressure–sensitivity factor $\mu$ ranges from 0.10 to 0.25 for polymers [13, 14]. The Drucker–Prager plasticity model with $\mu$ = 0.1 and $k$ = 43.30 MPa was used

to study of the matrix cracking damage mechanism. An associative flow rule is used to compute the direction of plastic flow [10].

(a)

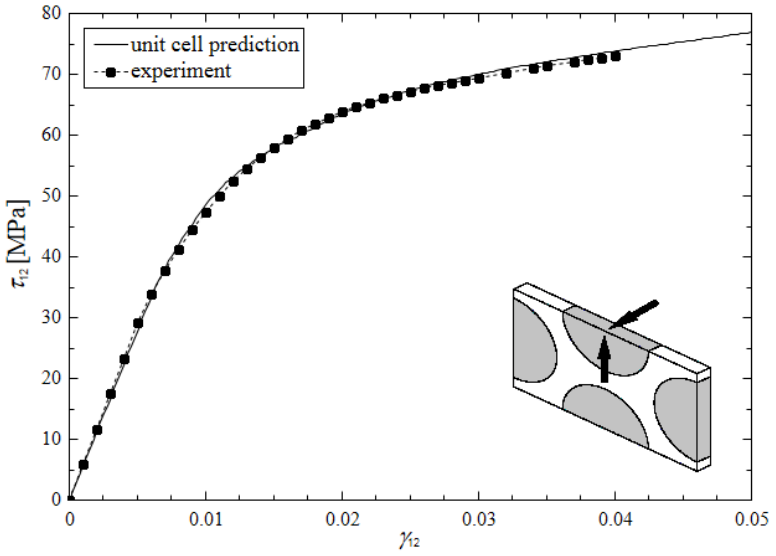


(b)

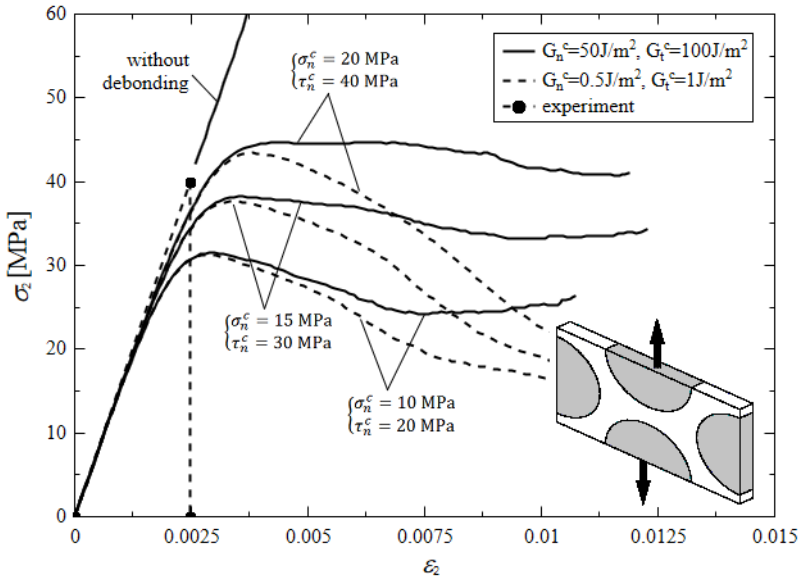


Figure 2: Calibration of the mesoscale model: (a) identification of the matrix plasticity model (experimental data from [9]), (b) identification of the fiber/matrix interface model (experimental data from [9]).

Experimental investigations of failure in transversely-loaded fiber-reinforced polymers have revealed that another damage mechanism is debonding occurring at the fiber/matrix interface [15,16]. For the fiber/matrix interface failure, a cohesive zone model is employed, in which the constitutive equations of the interface relate the normal $\sigma_n$ and tangential $\tau_t$ cohesive tractions to the normal $u_n$ and tangential $u_t$ displacement jumps and a scalar damage variable $d$, through [17]

$$\sigma_n = k_n u_n (1-d), \quad \tau_t = k_t u_t (1-d), \tag{5}$$

where $k_n$ , $k_t$ are initial contact stiffnesses in the normal and tangential direction, respectively. The variable $d$ represents the loss of stiffness and it is a function of both displacement jumps. The variable $d$ takes values from 0 to 1. Relationships (5) demonstrate linear elastic loading region followed by linear softening region. When $d = 0$, the cohesive elements are closed and the tractions increase linearly up to their maximum values $\sigma_n^c$, $\tau_t^c$ in the normal and tangential direction, respectively. When $0 < d < 1$, these elements begin to open and the tractions decrease linearly. When $d = 1$, the tractions are zero and the cohesive elements are completely broken. To define the completion of fracture in the cohesive zone model, a linear energy criterion is used [17]

$$(G_n / G_n^c) + (G_t / G_t^c) = 1, \tag{6}$$

(a)

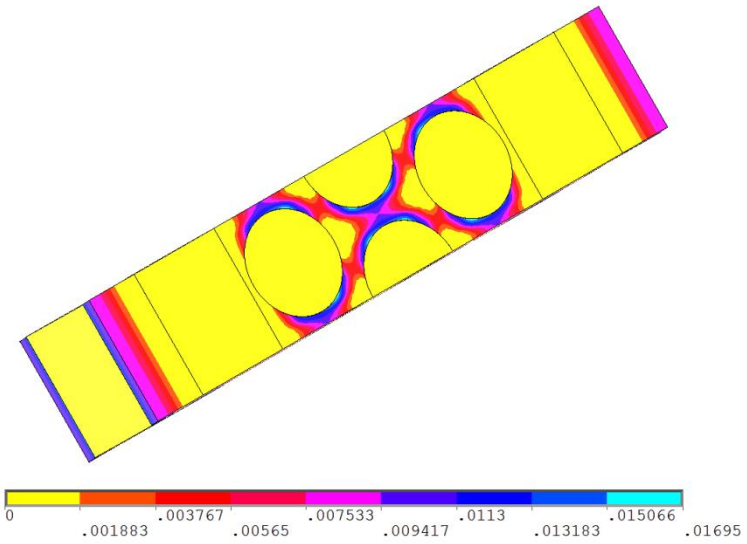


(b)

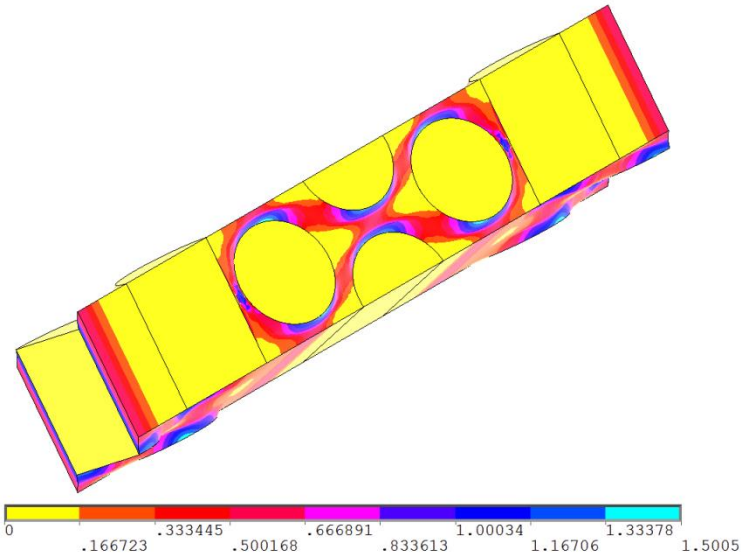


Figure 3: Contour plots of the effective plastic strain in the $\pm 45^o$ angle-ply laminate at the critical stage of deformation from the mesoscale model with (a) imperfect and (b) perfect fiber/matrix interface conditions.

where $G_n$, $G_t$ denote energy release rates for mode I fracture and mode II fracture, respectively and $G_n^c$ and $G_t^c$ correspond to the interfacial fracture energies. After debonding is complet-

ed, the interface surface interaction is governed by standard contact constraints for normal and tangential directions. A cohesive layer consisted of contact elements with eight nodes (CONTA174, TARGE170) was introduced between the fibers and the matrix to reproduce the fiber–matrix debonding. The glass fibers are assumed to be linear elastic.

### 2.3 Calibration of the Drucker–Prager plasticity model

In this paper, the hardening curve of epoxy matrix is extracted from a hexagonal unit cell subjected to in–plane shear loading. The non–linearity of epoxy matrix is identified such that prediction obtained from the hexagonal unit cell matches the measured in–plane shear response of E-glass/MY750 epoxy unidirectional lamina reported in [9]. Fig.2a shows a comparison of the measured shear response and that from the hexagonal unit cell model. Agreement with experimental data is quite good.

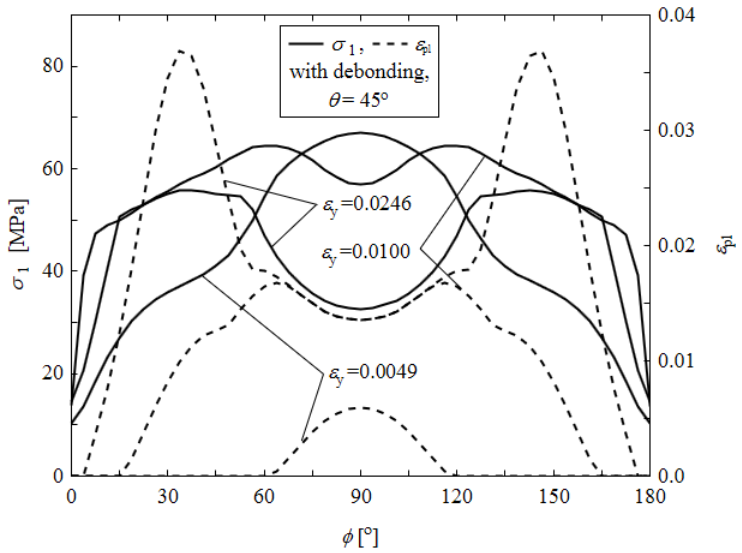


Figure 4: Angular distributions of the first principal stress and the effective plastic strain at the fiber/matrix interface at three successive stages of deformation from the mesoscale model with imperfect fiber/matrix interface.

### 2.4 Calibration of the interface model

In order to ascertain the cohesive properties for the interface under study, an analysis of debonding under transverse tension was carried out for various interfacial cohesive strengths and fracture energies. It was assumed that the ratio of the tensile interfacial strength to the shear interfacial strength, $\sigma_n^c / \tau_t^c$ and the ratio of the opening component to the sliding component of the interfacial fracture energy, $G_n^c / G_t^c$ are 0.5. The macroscopic tensile stress–strain curves calculated for four different levels of interfacial strength ($\sigma_n^c / \tau_t^c$ = 10/20, 15/30, 20/40 and ∞) and two different levels of interfacial fracture energy ($G_n^c / G_t^c$ = 0.5/1, 50/100) are shown in Fig.2b. It can be observed from this figure that an increase in the interfacial strength produces an increase in the transverse tensile strength of composite, and in turn, a decrease in the interfacial fracture energy leads to a larger decrease in macroscopic stress at the post critical stage. The strength of the interface under study was calibrated such that the peak of the transverse stress-strain curve obtained from the hexagonal unit cell matches the measured transverse tensile strength of the composite reported in [9]. Due to lack of experimental data on the softening behavior of the entire composite at the macroscale, the interfacial fracture energy was assumed to be of the same order of magnitude as that measured in single-

fiber tests reported in [18]. Finally, the interface with $\sigma_n^c$ =15MPa, $\tau_t^c$ = 30MPa, $G_n^c$ = 15J/m$^2$ and $G_t^c$ = 30J/m$^2$ was chosen for the rest of the study.

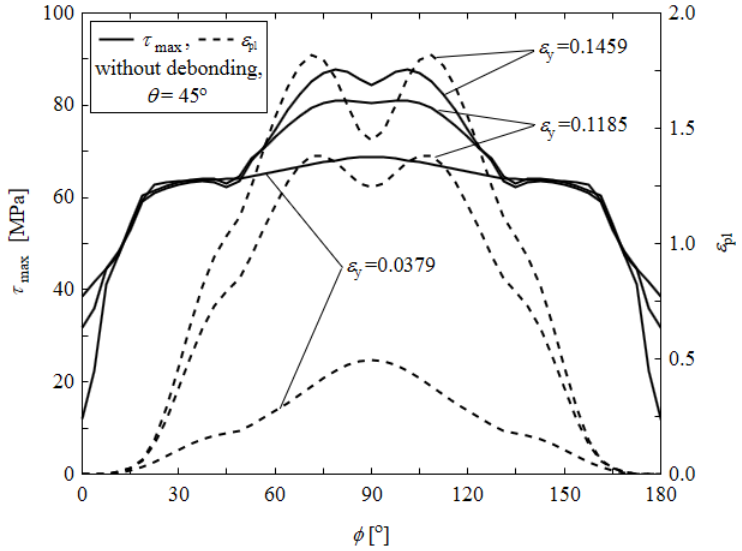


Figure 5: Angular distributions of the maximum shear stress and the effective plastic strain at the fiber/matrix interface at three successive stages of deformation from the mesoscale model with perfect fiber/matrix interface.

## 3 FAILURE MECHANISMS

Each ply in an angle-ply laminate subjected to tension is loaded by a combination of normal and shear stresses. The value of these stresses depends on the ply orientation angle $\theta$. Both shear and tensile loading modes can induce initiation and growth of cracks in the matrix along the fiber direction. For the sake of simplicity, an interaction between the two fracture modes is omitted in the present paper. In order to identify the failure mechanism of angle-ply laminates under tensile loading, an analysis of the local stresses in the unit cell models for different ply orientations is performed by the finite element method. For this purpose, it is assumed that the initiation of cracks in the matrix occurs if the maximum shear stress in the matrix or the first principal stress in the matrix goes beyond the corresponding ultimate strengths of the matrix

$$\tau_{max} \geq S_m, \quad \text{or} \quad \sigma_1 \geq Y_m. \tag{7}$$

Tension tests carried out on microscopic specimens indicate that the tensile strength of epoxy polymer $Y_m$ is much higher than that obtained with standard macroscopic specimens. The use of microscopic data is essential for the current analysis. According to works by Fiedler et al., [19], Hobbiebrunken et al. [20], the tensile strength of the epoxy polymer obtained from microscopic tests can exceed 100 MPa, while macroscopic tests yield the value of 80 MPa. To the author's knowledge, there are no micro-shear tests for epoxy polymers. The shear strength of the epoxy polymer $S_m$ obtained from macroscopic tests is 70 MPa [19, 20]. However, it is reasonable to assume that the true shear strength of the epoxy matrix is also higher. The shear strength of the epoxy matrix back-calculated from tension tests of the ±55 angle-ply laminate is 87 MPa [8].

## 4 RESULTS

Depending on the type of the fiber/matrix interface, two various mesoscale models of the ±45 angle-ply laminate were considered, namely models with the perfect and imperfect fiber/matrix interface conditions. Fig.3 shows distributions of the equivalent plastic strain in these models for critical loads. In the case of the imperfect interface, the critical load corresponds to a limit beyond which the fiber/matrix interface cracks are fully opened ($\varepsilon_y^c = 0.01$). In turn, in the case of the perfect interface, it corresponds to a limit beyond which the shear strength of the matrix is attained ($\varepsilon_y^c = 0.1185$). The most intense plastic deformation in the matrix is localized in shear bands which develop along planes containing the fiber direction. Thus, both models predict that cracking of the matrix takes place along the fiber direction within the shear bands.

(a)

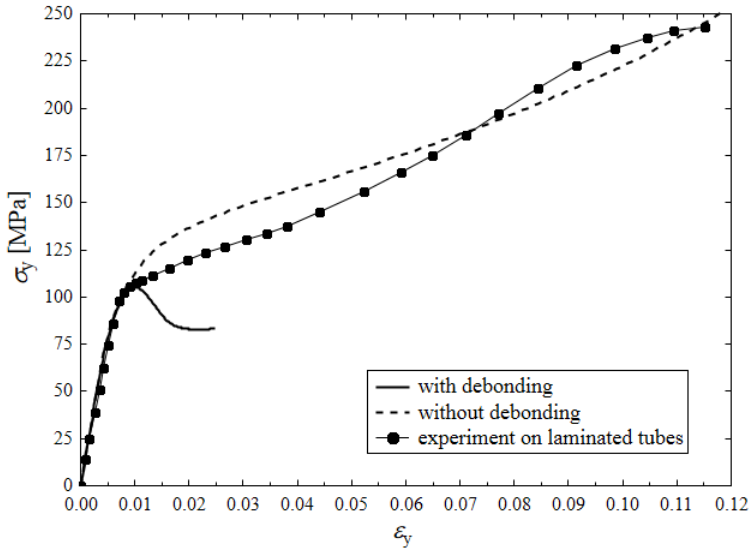


(b)

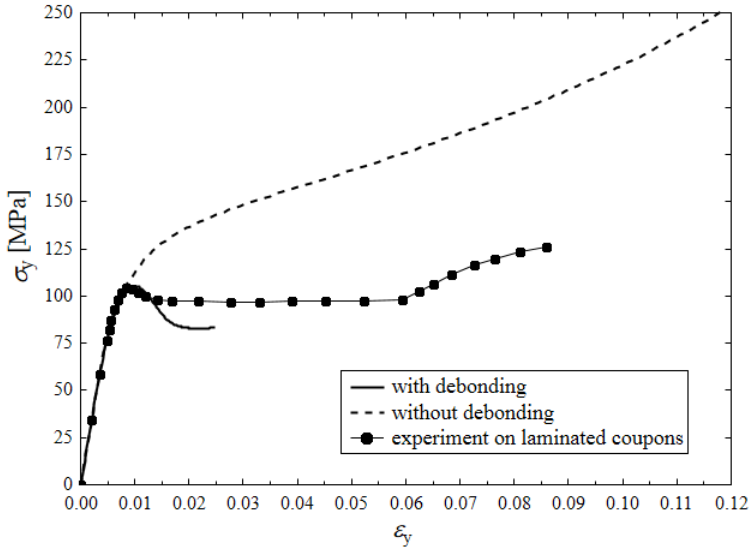


Figure 6: Comparison of the stress-strain curves of the ±45° angle-ply laminate obtained from different fiber/matrix interface conditions with experimental data: (a) tensile tests from [21] carried out on laminated tubes, (b) tensile tests from [22] carried out on laminated coupons.

In order to check the reliability of the opening mode of fracture, an analysis of the first principal stress $\sigma_1$ and the equivalent plastic strain $\varepsilon_{pl}$ in the matrix is performed by using the mesoscale model with the imperfect fiber/matrix interface. The distributions of these quantities at the fiber/matrix interface are presented in Fig.4 at three successive stages of deformation corresponding to the beginning of inelastic behavior, the limit load and the softening regime. The polar angle at the fiber/matrix interface $\phi$ is measured from the normal to the interlaminar interface. It is interesting to note that the tensile stress in the matrix decreases at the softening regime and it is below the tensile strength ($Y_m$ = 100 MPa). In contrast to the tensile stress, the plastic strain in the matrix increases constantly with increasing applied strain. This means that the condition for crack growth in the matrix under the opening mode of fracture cannot be satisfied.

In order to validate the shearing mode of fracture, an analysis of the maximum shear stress $\tau_{max}$ and the equivalent plastic strain $\varepsilon_{pl}$ in the matrix is performed by using the mesoscale model with the perfect fiber/matrix interface. The distributions of these quantities at the fiber/matrix interface are presented in Fig.5 at three successive stages of deformation. It can be observed in Fig.5 that both the shear stress $\tau_{max}$ and the plastic strain $\varepsilon_{pl}$ in the matrix increase with increasing applied strain. Thus, the shear stress in the matrix may go beyond the shear strength of the epoxy matrix ($S_m$ = 87 MPa). It is also interesting to note that the mesoscale model with the perfect fiber/matrix interface exhibits a very ductile behavior. At the critical stage of deformation, the plastic strain in the matrix exceeds 140% .

Predictions of the stress-strain behavior for the perfect and imperfect fiber/matrix interface conditions are shown in Figs.6a and 6b. Two different experimental curves reported in the literature [21-22] for the ±45 angle-ply laminate are included for quick reference in these figures. The two experimental curves of the ±45 angle-ply laminate show a very non-linear behavior prior to ultimate failure. This behavior is manifested by a hardening region at high strains. The observed increasing stiffness can be attributed to a rotation of fibers due to shear stress. As the ply shear stress increases, the matrix is plasticized and the orientation of the fibers became more aligned with the loading axis, which leads to an increase in load carried by fibers. The fibers are capable of carrying more load only if the displacement compatibility between matrix and fibers exists. Thus, the experimental curves of the ±45 angle-ply laminate obtained from both tests suggest that fiber-matrix debonding has a negligible influence on the deformation of this laminate under tensile loading. It can be observed in Fig.6a that the stress-strain curve obtained from the mesoscale model with the perfect fiber/matrix interface match quite well with experimental data. In turn, the experimental curve of the ±45 angle-ply laminate obtained from tests on laminated coupons exhibits a maximum and a plateau before a hardening region. It can be observed in Fig.6b that the maximum of the stress-strain curve obtained from the mesoscale model with the imperfect fiber/matrix interface overlaps with the maximum from the tests. Thus, this model may be used to predict the beginning of the plateau occurring during tensile tests carried out on laminated coupons.

## 5 CONCLUSIONS

The efficiency of two types of mesoscale models without and with fiber/matrix debonding for simulating the deformation and failure mechanisms in a ±45 angle-ply laminate under tensile loading was evaluated. The results from both models suggest that failure of the laminate is dominated by the matrix shearing. The first type was found to reproduce well the tensile response of the laminate obtained from laminated tubes, and in turn, the second type was able to predict the beginning of the plateau occurring during tensile tests carried out on laminated coupons.

## ACKNOWLEDGMENT

The financial support of the National Science Centre of Poland under contract DEC–2011/03/D/ST8/04817 is thankfully acknowledged.

## REFERENCES

[1] M. Herráez, D. Mora, F. Naya, C.S. Lopes, C. González, J. LLorca, Transverse cracking of cross-ply laminates: A computational micromechanics perspective. *Compos. Sci. Technol.*, **110**, 196–204, 2015.

[2] G. Soni, R. Singh, M. Mitra, B.G. Falzon, Modelling matrix damage and fibre–matrix interfacial decohesion in composite laminates via a multi-fibre multi-layer representative volume element (M2RVE). *Inter. J. Solids Struct.*,**51**, 449–461, 2014.

[3] W.H. Ng, A.G. Salvi, A.M. Waas, Characterization of the in-situ non-linear shear response of laminated fiber-reinforced composites. *Compos. Sci. Technol.*, **70**, 1126–1134, 2010.

[4] T, Matsuda, D. Okumura, N. Ohno, M. Kawai, Three-dimensional microscopic interlaminar analysis of cross-ply laminates based on a homogenization theory. *Int. J. Solids Struct.*, **44**, 8274–8284, 2007.

[5] Y. Zhang, Z. Xia, F. Ellyin, Viscoelastic and damage analysis of fibrous polymer laminates by micro/meso-mechanical modeling. *J. Compos. Mater.*,**39**, 2001-2022, 2005.

[6] Y. Zhang, Z. Xia, F. Ellyin, A 3D meso-scale amalysis of angle-ply laminates. *Mech. Adv. Mater. Struct.*, **20**, 801-810, 2013.

[7] F. Ellyin, Y. Zhang, Z. Xia, Meso-scale analysis of angle-ply laminates. *Proc. Eng.*, **10**, 63–68, 2011.

[8] M. Romanowicz, A mesoscale study of failure mechanisms in angle-ply laminates under tensile loading. *Composites Part B*, **90**, 45-57, 2016.

[9] P.D. Soden, M.J. Hinton, A.S. Kaddour, Lamina properties, lay-up configurations and loading conditions for a range of fibre-reinforced composite laminates. *Compos. Sci. Technol.*, **58**, 1011–1022, 1998.

[10] Ansys. *Theory reference for the mechanical APDL and mechanical applications*, Release 14.1. Canonsburg PA: Ansys, 2012.

[11] Z. Xia, Y. Zhang and F. Ellyin Unified periodical boundary conditions for representative volume elements of composites and applications. *Int. J. Solids Struct*., **40**, 1907–1921, 2003.

[12] D.C. Drucker, W. Prager. Soil mechanics and plastic analysis for limit design. *Q. Appl. Math.*, **10**, 157–165, 1952.

[13] A.J. Kinloch, R.J. Young, *Fracture behavior of polymers*. Netherlands: Elsevier, 1983.

[14] R. Quinson, J. Perez, M. Rink, A. Pavan, Yield criteria for amorphous glassy polymers. *J. Mater. Sci.*, **32**, 1371–1379, 1997.

[15] B. Fiedler, C. De Jong, T. Hobbiebrunken, M. Hojo, K. Schulte, Micro/macro-mechanical approach of first ply failure in CFRP. *J. Mater. Sci.*, **41**, 6760–6767, 2006.

[16] D.C. Foster, G.P. Tandon, M. Zoghi, Evaluation of failure behavior of transversely loaded unidirectional model composites. *Exp. Mech.* **46**, 217–243, 2006.

[17] G. Alfano, M.A. Crisfield, Finite element interface models for the delamination analysis of laminated composites: mechanical and computational issues. *Int. J. Numer. Method. Eng.*, **50**, 1701–36, 2001.

[18] J. Varna, L.A. Berglund, M.L. Ericson, Transverse single-fibre test for interfacial debonding in composites: 2. Modelling. *Composites Part A*, **28**, 317–26, 1997.

[19] B. Fiedler, M. Hojo, S. Ochiai, K. Schulte, M. Ando, Failure behavior of an epoxy matrix under different kindsof static loading. *Compos. Sci. Technol.*, **61**, 1615–1624, 2001.

[20] T. Hobbiebrunken, B. Fiedler, M. Hojo, M. Tanaka, Experimental determination of the true epoxy resin strength using micro-scaled specimens. *Compos Part A*, **38**, 814–818, 2007.

[21] F.A.R. Al-Salehi, S.T.S. Al-Hassani, M.J. Hinton, An Experimental investigation into the strength of angle ply GRP Tubes under High Rate of Loading. *J. Compos. Mater.* **23**, 288-305, 1989.

[22] A. Rotem, Z. Hashin, Failure modes of angle ply laminates. *J. Compos. Mater.*, **9**, 191-206, 1975.